ATLANTIS PRESS

Atlantis Highlights in Engineering, volume 4

13th International Renewable Energy Storage Conference (IRES 2019)

Topology and Efficiency Analysis of Utility-Scale Battery Energy Storage Systems

Anupam Parlikar*, Holger Hesse†, Andreas Jossen‡
Institute for Electrical Energy Storage Technology (EES), Technical University of Munich (TUM)
Munich, Germany
Email: *anupam.parlikar@tum.de, †holger.hesse@tum.de, ‡andreas.jossen@tum.de

***Abstract*—Energy storage is an important flexibility measure to stabilize and secure the electrical energy supply system. Lithium-ion battery energy systems (BESS) are, owing to their characteristics, uniquely poised to support and augment the functioning of the energy supply system. It is crucial to identify and analyze the factors which play a role in their efficient and effective operation. This paper identifies and analyses three such major factors - application scenarios, power electronics with power distribution strategies, and battery parameters which influence the efficiency of a BESS. The applications analyzed are primary control reserve and peak shaving. Two Power electronics topologies and their load distribution strategies are presented, with their influence on the conversion efficiency being evaluated subsequently. Two commercial lithium-ion technologies - a Lithium Iron Phosphate cathode/Graphite anode cell and a Lithium Nickel Manganese Cobalt Oxide cathode/Graphite anode cell are also simulated for two states of health (SOH). The aged cells are considered to possess a capacity equal to 80% of original nominal capacity and a cell resistance twice that of the new cells. It is found that the system conversion efficiency can be greatly improved in applications with low active charge-based and high temporal utilization ratios by deploying a suitable power electronics topology and load distribution strategy. For applications with high active charge-based and low temporal utilization ratios, the battery resistance and the serial-parallel combination play an important role.**

***Index Terms*—energy storage, lithium-ion battery, efficiency, battery energy storage system**

I. Introduction

With the global advent of cost-competitive electricity produced by fluctuating renewable energy sources such as photovoltaic solar and wind turbines [1]–[3], the economic hurdles in the way of large-scale adoption of these technologies are set to gradually disappear. At the same time, increasing grid-penetration ratios pose significant challenges to the maintenance of grid stability and power quality [4], [5]. A variety of flexibility options will have to be pressed into service to be able to smooth out the mismatch between load and demand at all times [6]. Energy storage, being one such flexibility measure, is slated to play a pivotal role in the stabilization of the grid in the upcoming times [7].

Stationary Lithium-ion battery energy storage systems (BESS) are increasingly being seen as a reliable solution to the challenge posed by the acute requirement of flexibility measures aiding the grid to maintain its stability. Stationary BESS can provide a number of vital ancillary services to the electricity supply system such as - frequency control, voltage control, load balancing, peak shaving, among others [8]–[11]. Lithium-ion BESS technology is the leading battery energy storage technology in current times owing to its relatively high round-trip efficiency, high energy and power density as well as superior lifetime performance [10], [12].

This paper aims to highlight some of the factors influencing the efficiency of a stationary BESS. Section II discusses the components of a modern stationary BESS and the influence of components on the efficiency of the system. This is followed by section III, in which definitions of performance indicators employed in this paper are presented. Section IV-A discusses the dependence of the efficiency on the kind of service being provided by a BESS, with a further focus on two grid-related applications. The section IV-B discusses the influence of the cells used on the system efficiency, whereas the subsequent section IV-C investigates the influence of the power electronics components on the efficiency of the system.

II. State-of-art

A typical stationary BESS, depicted in fig. 1, generally comprises of the following sub-components [9], [13]:

1) Battery system:
   a) Cell
   b) Module
   c) Rack
2) Power Electronics
   a) DC/DC converter(s)
   b) AC/DC converter(s)
3) Auxiliary components
   a) Energy Management System (EMS)
   b) Battery Management System (BMS)
   c) Thermal Management System (TMS)

The individual lithium ion cells are combined in series to form strings, two or more of which are combined in parallel to form modules. These modules are further combined as per requirements to yield racks or packs at the desired voltage level. The power electronics come into the picture at this stage, where a DC/DC converter can used to further step up the DC terminal voltage of the rack/pack before being connected to an AC/DC converter that then interfaces with the grid, depending on the voltage level, either directly, or with a transformer in between. The DC/DC converter is often optional, but when used it enables the battery system to be

used across a wider range of its voltage curve, as lower terminal voltages can also be stepped up to match those required by the AC/DC converter. This greater usable range comes at the cost of efficiency losses across the DC/DC converter, which, depending on the particular system, might be acceptable in light of the wider operating voltage range. The DC/DC converter and transformer are not considered further in this work. The energy conversion processes that enable the

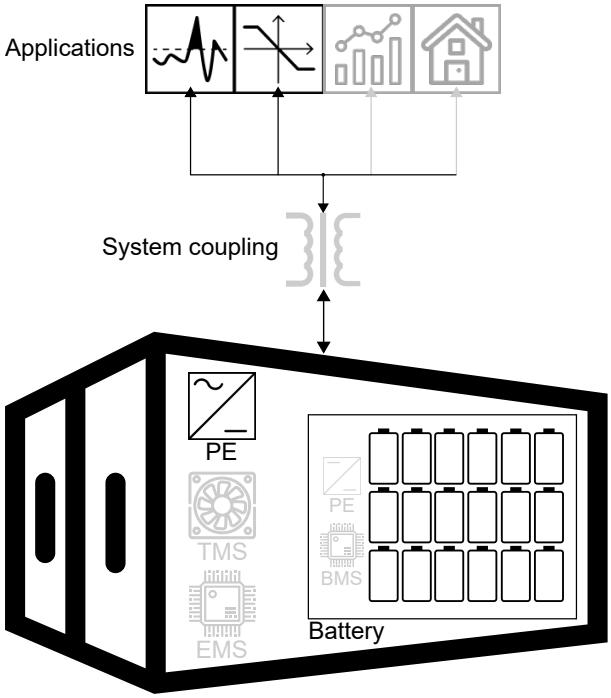

Fig. 1: Schematic diagram of a typical stationary battery energy storage system (BESS). Greyed-out sub-components and applications are beyond the scope of this work.

storage of electrical energy in the form of chemical energy take place within the power electronics and the battery system. The energy management, battery management, and thermal management systems can be termed as auxiliary components, and are responsible for controlling and ensuring the safe operation of the BESS. The large portion of losses in the first two components are the conversion losses. The remaining losses such as the standby losses and consumption by other components constitute the system losses. Schimpe et al [14] present a further breakdown of the conversion losses and system losses into detailed individual loss mechanisms within each sub-system. They list a total of 18 loss mechanisms, and present a detailed analysis with the help of an electro-thermal modeling framework. It is found that the conversion losses in the power electronics and the battery system are significant. The framework is based on the results of a container BESS named *Energy Neighbor* [15], developed at the Technical University of Munich as part of a research project *EEBatt*. Patsios et al [16] also confirm that the conversion losses in the battery system and power electronics) are significant and warrant a closer look. Not only does the the choice of size, layout and operating strategy of sub-components play an important role in application in determining the overall round-trip efficiency of the system, but also the service being rendered by a BESS [17]. This paper highlights the relation between the conversion losses and aspects such as the application scenario and system configuration. Evaluation of system losses (such as standby losses, power consumption by auxiliary components) is not a part of this work.

III. Definitions of performance indicators

In this section, definitions of performance indicators used in the subsequent sections of this paper are presented.

A. Efficiency

The efficiency (η_{system}) of a battery energy storage system is defined as the ratio of the time integral of the discharging power to the time integral of the charging power over a complete cycle such that the initial and final states of charge (SOCs) are identical [14]. The system necessarily encounters dissipative losses at all times in all the components, and especially during the charge and discharge processes. The value of η_{system} therefore, lies between 0 and 1, as the discharged energy is always less than the charging energy.

$$\eta_{system} = \frac{\int_0^{t_1} P_{discharge}(t) \cdot dt}{\int_{t_1}^{t_2} P_{charge}(t) \cdot dt}\Bigg|_{SOC_0=SOC_{t_2}} \tag{1a}$$

$$= \frac{E_{discharged}}{E_{charged}}\Bigg|_{SOC_0=SOC_{t_2}} \tag{1b}$$

$$E_{charged} = E_{discharged} + E_{loss,total}\Big|_{SOC_0=SOC_{t_2}} \tag{1c}$$

$$E_{loss,total} = \sum_{i=1}^{n} E_{loss,c,i} + \sum_{i=1}^{n} E_{loss,s,i}\Big|_{SOC_0=SOC_{t_2}} \tag{1d}$$

where:
.. η_{system} is the system efficiency
.. $E_{discharged}$, $E_{charged}$ represent the energy discharged and charged respectively
.. $E_{loss,c/s,i}$ represents the energy lost in the ith component due to conversion (c) and system (s) losses respectively
.. n is the total number of components for which the losses are evaluated
For the purpose of this work, only the conversion losses are considered, i.e. it is assumed that the sum of system losses $\Sigma E_{loss,s,i}$ is effectively zero. This assumption implies that the efficiency definition applied in this paper refers to the conversion efficiency of the system.

B. Temporal utilization ratio

The temporal utilization ratio τ_t is defined in [14] as the ratio of the sum total of the time during which the BESS is in operation to the total time of the simulation. This indicator is particularly useful to compare load profiles against each other with respect to the degree of activity seen by a BESS.

The quantity τ_t can therefore assume values between 0 and 1, depending on how often the system is summoned into service.

$$\tau_t = \frac{t_{operation}}{t_{simulation}} \tag{2a}$$

where:
.. τ_t is the temporal utilization ratio
.. $t_{operation}$ is the total time of operation of the BESS
.. $t_{simulation}$ is the duration of simulation

C. Active charge-based utilization ratio

The active charge-based utilization ratio $\tau_{Q,a}$ is defined as the ratio of sum of absolute values of charge throughput of the BESS in charge and discharge directions during the non-idle time periods to the sum of the absolute charge throughout in the two directions at a C-rate of 1 C within the same periods. A C-rate of 1 is that value of current which can completely charge/discharge a battery in a duration of 1 hour. The quantity $\tau_{Q,a}$ provides an indication of how demanding a particular load profile is with respect to the battery capacity. In contrast to the temporal utilization ratio τ_t, the active charge-based utilization ratio $\tau_{Q,a}$ is useful to compare load profiles against each other with respect to the intensity of activity demanded of a BESS. From the definition, it is then clear that $\tau_{Q,a}$ may assume a value between 0 and the sum of maximum permissible charge and discharge C-rates. Schimpe et al [14], on the other hand, present a related performance indicator which compares the actual battery charge throughput to that due to cycling the battery continuously at 1C throughout the duration of simulation.

$$\tau_{Q,a} = \frac{Q_{throughput}}{\tilde{Q}_{throughput,1C}} \tag{3a}$$

where:
.. $\tau_{Q,a}$ is the active charge-based utilization ratio
.. $Q_{throughput}$ is the total absolute charge throughput of the BESS
.. $\tilde{Q}_{throughput,1C}$ is the theoretical total absolute charge throughput of the BESS at 1C

D. System availability

In the discipline of systems engineering, the system availability and reliability are measures to quantify the likeliness of the system operating as expected under the given service conditions in a time frame of interest. It quantifies the actual performance of the system vis-a-vis its expected performance. The BESS may fail to perform as expected in cases wherein the C-rates, SOC values or temperatures tend to step out of the permissible range. The system may also reject requests in the case of failure/degradation of components resulting in impaired or zero capabilities [18]. Here we define two sub-indicators under this category:

1) Qualitative system availability: The qualitative system availability $s_{qualitative}$ is defined as the ratio of the number of successfully completed energy requests (charge, discharge, or both) to the total number of requests made to the BESS within the time frame of interest. This quantity can assume values between 0 and 1.

$$s_{qualitative} = \frac{n_{fulfilled}}{n_{requested}} \tag{4a}$$

where:
.. $s_{qualitative}$ is the qualitative system availability factor
.. $n_{fulfilled}$ is the number of energy service requests (charge, discharge or both) successfully fulfilled by the system
.. $n_{demanded}$ is the total number of energy service requests (charge, discharge, or both) received by the BESS

2) Quantitative system availability: The quantitative system availability factor is defined as the ratio of the actual quantity of energy exchanged (charge/discharge, or both) with the energy supply system to the quantity of energy exchange requested within the time frame under consideration. This ratio can assume values between 0 and 1, implying complete incapability and total fulfillment respectively. Values in between point to partial fulfillment.

$$s_{quantitative} = \frac{E_{fulfilled}}{E_{requested}} \tag{5a}$$

where:
.. $s_{quantitative}$ is the quantitative system availability factor
.. $E_{fulfilled}$ is the actual energy service (charge, discharge or both) fulfilled by the system
.. $E_{demanded}$ is energy service (charge, discharge, or both) requested of the BESS
For grid applications such as peak shaving, the request to discharge is of prime interest, and the system availability of a BESS providing such a service would be based on the number of discharge requests successfully honored. For other applications such as primary control reserve (PCR), the requests to both charge as well as discharge the system in response to frequency fluctuations are of interest, and the system would be mandated to fulfill all requests with a system availability of 1, in order to stay within the regulatory bounds.

IV. Factors influencing efficiency

To illustrate the dependence of the conversion efficiency on the system configuration and the application scenario in which the system is operated, simulations are run with the stationary battery energy storage system simulation tool SimSES [19], which has been developed at the Technical University of Munich. The definition of efficiency presented in the section III, and especially the conversion efficiency is used in evaluations presented in the subsequent sections.

A. Application scenario

Two applications of large-scale stationary BESS in the electrical energy supply system are considered to highlight

the dependence of conversion losses on the characteristics of the application. The applications considered are:

1) Peak Shaving (PS)
2) Primary Control Reserve (PCR)

The peak shaving (PS) application is known to subject the BESS to infrequent bursts of high-intensity energy requests, whereas the primary control reserve (PCR) application is the opposite in the sense that it subjects the BESS to frequent low-intensity energy requests throughout the time frame of consideration. In summary, the PS application exhibits a low τ_t and a high $\tau_{Q,a}$ value, while on the contrary, the PCR application exhibits a high value of τ_t and a low value of $\tau_{Q,a}$. In applications that exhibit high $\tau_{Q,a}$ values, the conversion losses in the batteries tend to be higher, whereas applications with simultaneously high τ_t and low $\tau_{Q,a}$ tend to suffer disproportionately high conversion losses in the power electronics, which fare sub-optimally under part-load conditions.

Two base case systems are defined to simulate BESS operation in the peak shaving and primary control reserve applications. The system configuration considered for each case is listed in table I. The voltage at the battery system terminals is 650 V in each case. The battery system is then connected to a bi-directional AC/DC converter whose DC operating range is 600-750 V. The system is then interfaced to the 400 V AC distribution grid. The system layout is described as ns mp, implying n cells in series, and m such combinations of n cells connected in parallel. This layout scheme is depicted in figure 2. The two applications chosen serve to underline

TABLE I: BESS system parameters

	Scenario	
	Peak Shaving	Primary Control Reserve
Energy capacity	350 kWh	2.8 MWh
Power rating	700 kW	1.4 MW (qualified)
Power Electronics	AC/DC bidirectional	AC/DC bidirectional
Cell chemistry	LFP/C	LFP/C
Form factor	Cylindrical 26650	Cylindrical 26650
System layout	204s 179p	204s 1430p
Cell state	New	New

the influence of the application on the individual components of the system conversion efficiency. A one size fits all design ideology is, hence not suitable for the deployment of stationary BESS in grid applications. The following sections depict how each application requires a BESS system design which is sensitive towards the unique demands of the application.

1) Peak Shaving: Deployment of battery energy storage systems to provide the so-called peak shaving service is fast gaining ground. Industrial and other commercial users with very high intermittent load peaks are required to not just pay for the amount of energy consumed, but also for the maximum power demand at their sites in their annual or monthly billing cycles. In order to avoid high power-related costs, peak shaving is a frequently implemented solution [20].

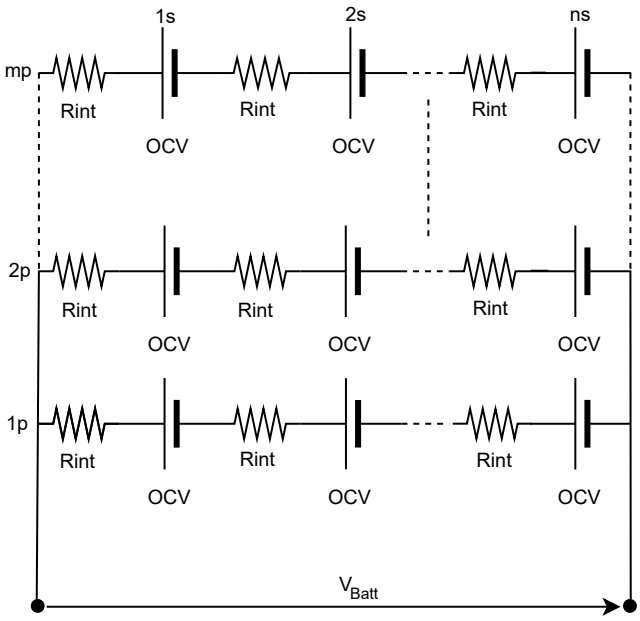

Fig. 2: System layout with n cells in series and m such strings in parallel (ns mp). OCV stands for open circuit voltage and Rint stands for internal resistance. Each cell is modelled as a voltage source with a series resistance.

Mature fossil-based technologies such as diesel generators and gas turbines installed on-site (captive power plants) are being replaced by BESS, owing to their precise and accurate response to demand, low response times, suitable ramp rates and relatively high efficiencies [10], [12]. These demand peaks are shaved off by the BESS at relatively higher C-rates than those normally witnessed in the PCR application. The BESS then charges in idle periods with relatively low C-rates. The operator of the peak shaving BESS can thus save costs related to the maximum power demand, and must only pay for the energy extracted from the grid at lower values of power [21]. While the motivation for peak shaving is often economic in nature, such systems can be also be used for strengthening of grid infrastructure at locations with disproportionately high intermittent loads such as at electric vehicle (EV) fast-charging stations, or to provide relief to a strained local distribution grid. All such systems reduce the peak instantaneous power demand that the grid has to fulfill, and spreads it over a larger period of time [22], [23].

For the purpose of this work, a synthetic load profile based on that of an industrial client is created with a high number of sharp peaks per day. The operation of the system described in table I is simulated for one year with a sample rate of 5 minutes in the exemplary peak shaving application. The peak load is 1.31 MW, while the minimum load is 95 kW. The average load during the simulated period is 211.69 kW. The temporal utilization ratio of this profile is 0.1930, meaning that the system is active for 19.30% of the simulated period. The grid connection to this load center, owing to specific

constraints, can only supply a maximum power of 630 kW. The BESS is operated in this scenario such that it caters to the residual demand over and above what the grid connection can supply. This limit, 630 kW in this case is termed as the peak shaving limit. The system operates within a C-rate range of 1 C for charging and 1.8867 C for discharging. The simulation results also reveal that the system is able to shave the peaks off by supplying the demanded power with a qualitative and quantitative system availability of 1 (i.e. 100%). An evaluation of the active charge-based utilization ratio reveals that the system operates with a $\tau_{Q,a}$ of 0.6961, which is relatively high. The conversion losses of the system over the simulated duration of one year are depicted on the right side in figure 4. It is clear that the conversion losses in the battery are significant and make up the largest proportion of losses in this application. While the conversion losses in the power electronics are comparable, there is not much room for improvement as the system operates near its rated capacity for a large portion of the operating time as shown on the left side of figure 3.

2) Primary Control Reserve: Operation of stationary BESS in provision of primary control reserve with consideration of its unique requirements has been investigated in scientific circles [24]–[28]. To simulate the operation of a stationary BESS in the PCR application, certain regulatory conditions have to be fulfilled. The minimum permissible energy capacity to power (E/P) ratio is governed by the regulatory framework to ensure guaranteed system readiness to provide a minimum prescribed duration of positive and negative reserves. A theoretical minimum ratio of 1 is required to fulfill the 30-minute criterion prescribed by the ENTSO-E (European Network of Transmission System Operators for Electricity) [29], but this ratio is not practically viable, as the storage system cannot charge or discharge energy at this ratio. An E/P ratio of 2 is therefore chosen to simulate the operation of a BESS in the PCR application. For such a system, the permissible SOC range in which the BESS may operate is then 25 - 75 %. Based on the grid frequency time series for the year 2017, the stationary BESS demand power profile is developed (see fig. 3). This profile has a temporal utilization ratio τ_t of 0.7999, which implies that the system remains in active operation for nearly 80% of the considered time period. In comparison to the temporal utilization ratio of around 19% for the PS application, the system is used much more frequently in the PCR application.As the grid frequency signal does not show any strong patterns, the BESS operation is simulated for the 15^{th} of each month of 2017, based on the frequency fluctuations and requested system response. The sample rate of these simulations is 1 second. The conversion efficiencies for the system described in table I are evaluated for the 12 sample days.

Figure 5 depicts the conversion losses in the power electronics and the battery system for the simulated days in 2017. Two cases are picked from these results for further discussion - the simulated sample days with the best and worst power electronics conversion efficiencies. The best conversion efficiency among the 12 sample days is observed on the 15^{th} of November, and the worst is observed on the 15^{th} of July, with the average value lying between them. From the C-rate distributions depicted in figure 5 for the 15^{th} of November (bottom right) and the 15^{th} of July (bottom left), it can be inferred that the BESS undergoes cycling under very gentle conditions in the PCR application. With a temporal utilization ratio τ_t of 0.8528 and active charge-based utilization ratio $\tau_{Q,a}$ of 0.0319, the simulation for the 15^{th} of November sees conversion losses of around 19% in the power electronics. On the other hand, with a τ_t of 0.7104 and a $\tau_{Q,a}$ of 0.0206, the conversion losses in the power electronics are nearly 29% on the 15^{th} of July. The system is operated under part-load conditions in both the cases for most of the time. Part-load operation at low C-rates while leading to low conversion losses in the battery system due to low currents flowing through the internal resistance, also implies higher losses in the power electronics components, which exhibit best conversion efficiencies at their nominal power ratings. The above results can also be explained from the C-rate distributions of the simulation for the 15^{th} of November, which has a higher average C-rate as compared to the simulation for the 15^{th} of July, which exhibits a lower average C-rate in the simulated time period. The two system availability ratios remain at 1 (100%) in all the sample days, indicating satisfactory performance of the system. It can thus be inferred that the power electronics conversion efficiency improves with rising values of $\tau_{Q,a}$. This was also apparent from the section on peak shaving, in which the system exhibited a very high value of active charge-based utilization ratio.

B. Battery system

From the results presented in subsection IV-A1 on the applicability of batteries in the peak shaving application, it is clear that the conversion losses in the battery play an important role in applications with relatively higher C-rates. To investigate the dependence of these losses on the cell parameters such as resistance and the cell capacity, three additional scenarios are simulated. In addition to the LFP/C 26650 cell, a commercial NMC/C 18650 cell is also simulated. Both the cell types are simulated twice - once considering the cells as 'new' - i.e. with 100% capacity and low internal resistance, the second set of simulations treats the cells as 'old' with only 80% of capacity and twice the internal resistance as compared to the new cells. For around 20% capacity loss, the resistance rise for the LFP/C cells is around 70% [30], while the resistance rise for the NMC/C cells is around 85% [31]. The assumption of 100% rise considered here is taken as a worst case scenario. Based on the objectives of the investigation, the use of various battery models such as empirical models, physico-chemical models and equivalent circuit models is prevalent [33]–[36] in scientific circles. Physico-chemical models are the closest to the underlying electrochemical processes taking place within the cell, whereas the equivalent circuit models, although quite popular in their usage, present a higher degree of abstraction, employing electrical circuit analogies to approximate

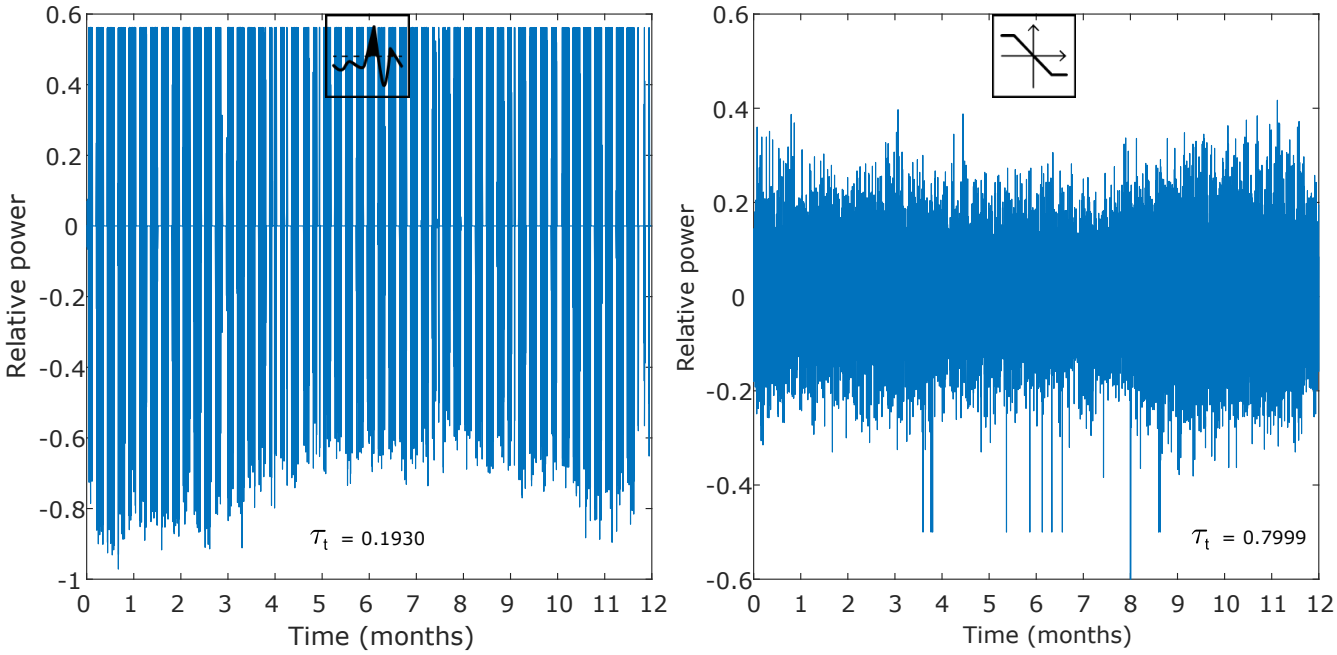

Fig. 3: Power profiles for the peak shaving (left) and primary control reserve (right) and applications (normalized with respect to the respective system power ratings).

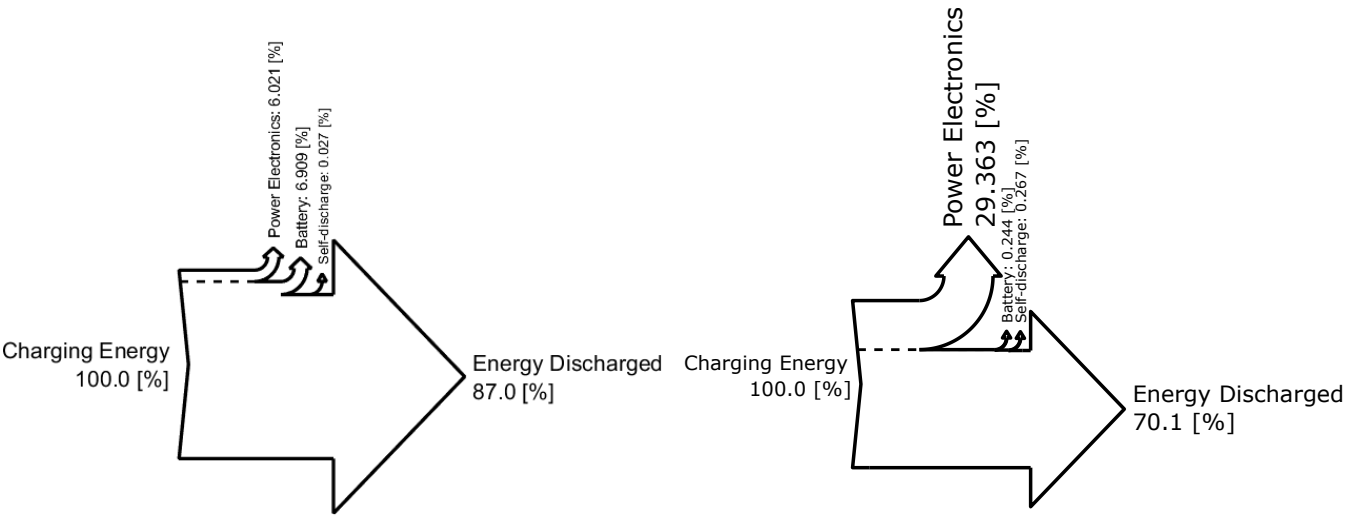

Fig. 4: Conversion losses in peak shaving (left) and primary control reserve (right) applications.

the physical processes. The empirical and data-based models are the farthest away from physical reality and are purely mathematical in nature.

1) Equivalent circuit model: As the dynamic response of the cell under load is not of prime interest in these analyses, the so-called Rint [36], [37] equivalent circuit model is deemed sufficient to assess the losses in the cells. The Rint model visualizes the battery as a series combination of a resistance with a voltage source (which represents the open circuit voltage). The values of the open circuit voltage are read out from a look-up table depending on the state of charge. The values of the internal resistance are also read out from look-up tables depending on the direction of power flow, the temperature and the state of charge. The open circuit voltage curves for both the cells and the Rint model (inset) are depicted in figure 6. The cell model (open circuit voltage and resistances) is scaled up to the module and rack level with the help of scaling factors. A number of commercial lithium-ion cells have been characterized and tested in the scientific community to model their electro-thermal and aging behavior with sufficient

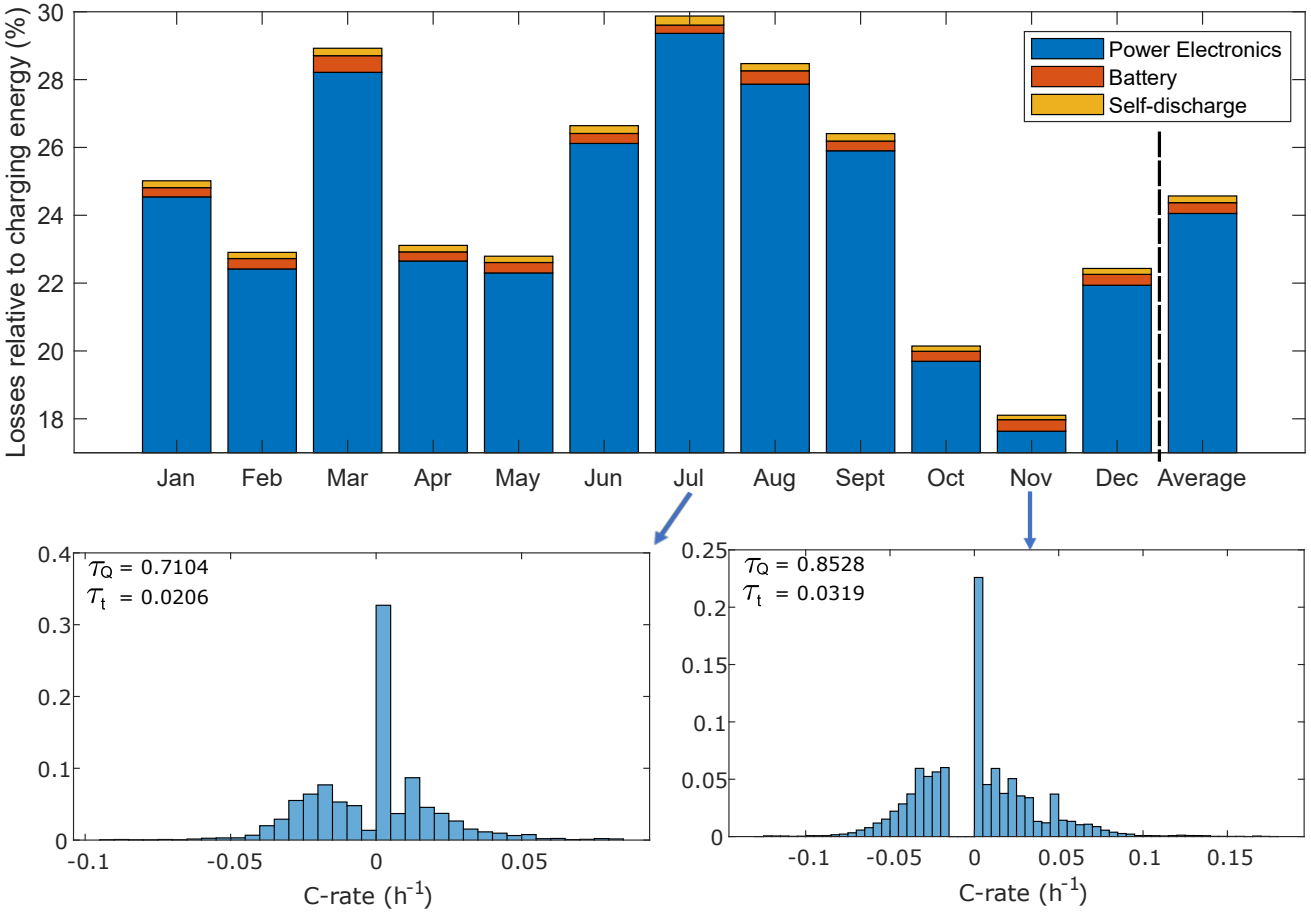

Fig. 5: Conversion losses during operation in PCR application (top). Distribution of system C-rates on 15 July (bottom left). Distribution of system C-rates on 15 November (bottom right).

accuracy [38]–[41]. The simulations carried out in this paper use two Rint equivalent circuit battery models (ECM) based on full cell characterizations of the LFP 26650 [19], [42], [43], and the NMC 18650 [31] cells. The dependence of the resistance of the LFP cells on the temperature and state of charge in the process of charging and discharging is depicted in figure 6. The dependence of the NMC cell resistance on the state of charge is also depicted in figure 6.

2) 0D lumped parameter thermal model: In conjunction with the Rint ECM model, the thermal behavior of the system is modeled as a 0D lumped parameter model at the cell level, and scaled up to the system level. The heat transfer processes considered include the internal heat generation on account of the dissipative losses in the internal resistance, and the heat exchange with the ambient air. The reversible heat exchanges due to the chemical reactions is not taken into account. The heat exchange with the ambient air is modeled as natural convection. The rise in temperature can be obtained from the energy balance equation for these two processes:

$$\Delta T = (\dot{Q}_{loss} + A \cdot h \cdot (T_{amb} - T_1))/(m \cdot c_p) \quad (6a)$$

$$T_2 = T_1 + \Delta T \quad (6b)$$

For the NMC/C cells in the peak shaving operation, the system configuration is 181s 276p for the same system energy and power ratings as the base case system. The number of cells in series is lower than in the LFP/C based system due to the higher open circuit voltage of the NMC/C cells. Due to the lower capacity of the NMC/C cells, it is imperative that a greater number of strings be connected in parallel as compared to the LFP/C case. Although the NMC/C cells exhibit resistance values which are higher, due to the difference in the system layout - 204s 179p for LFP/C vs. 181s 276p for NMC, the simulations reveal that the system with NMC/C cells sees a lower proportion of conversion losses in the battery system due to lower equivalent resistance values. It is seen from fig. 7 that the aged cells with lower capacities and higher resistances show a higher proportion of conversion losses in the battery. The self-discharge in proportion is negligible over the simulated period, as lithium-ion batteries in general exhibit favorable self-discharge characteristics. The conversion losses take the form of heat dissipation, and entail additional efforts to expel the heat out of the vicinity of the battery in order to keep it within its recommended temperature limits. The heating effect also causes faster aging of the cells, which

TABLE II: Cell parameters. 'n' stands for new, and 'a' stands for aged. (* approximate values from literature, further investigation necessary [32].)

	Cells			
	LFP-n	LFP-a	NMC-n	NMC-a
Charge capacity (As)	10800	8640	7020	5616
Max. continuous charge current (A)	3	3	1.95	1.95
Max. continuous discharge current (A)	20	20	3.9	3.9
Max. charge voltage (V)	3.6	3.6	4.2	4.2
Min. discharge voltage (V)	2	2	3	3
Mean internal resistance at 25°C (mΩ)	47.5	95	67.1	134.2
State of health (SOH)	100%	80%	100%	80%
Mass of cell (g)	85	85	47.5	47.5
Surface area (m^2)	0.0064	0.0064	0.0037	0.0037
Heat transfer coefficient (W/m^2K)	15	15	15	15
Specific heat capacity coefficient (J/kgK)	925.52	925.52	823*	823*
Form factor	26650	26650	18650	18650

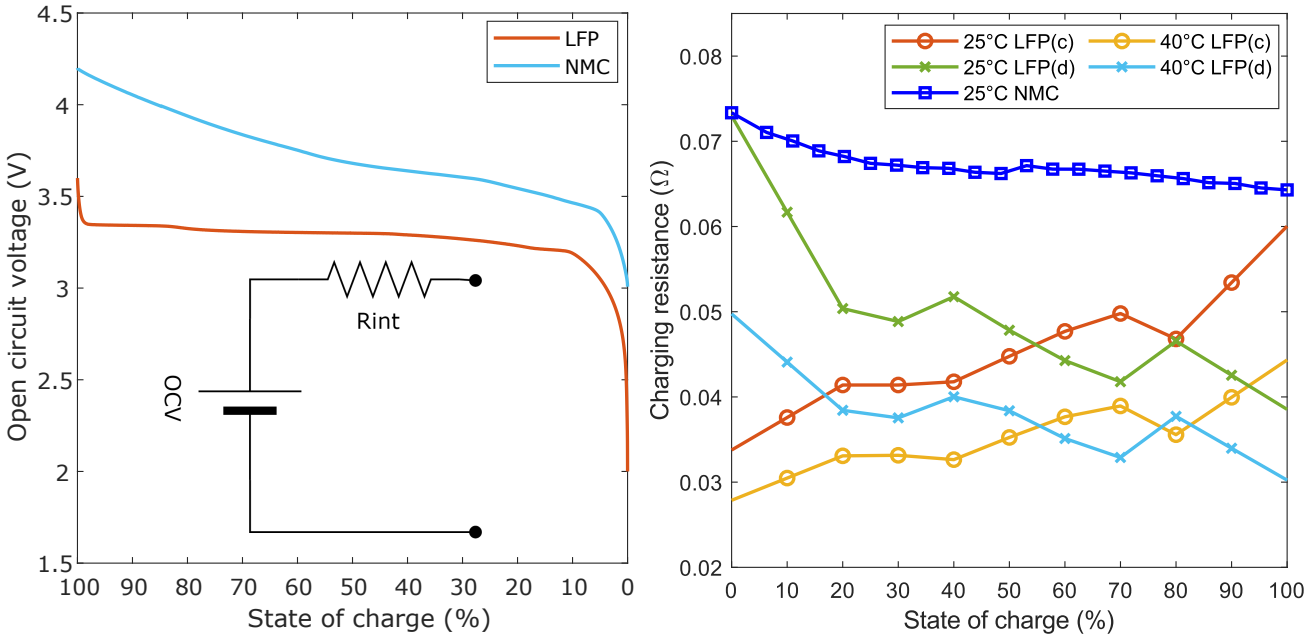

Fig. 6: Open circuit voltage curves (left) for the the LFP/C and NMC/C cells, with a schematic of the Rint cell model (inset). Dependence of ohmic resistance on state of charge and temperature (right). The symbols in brackets c and d stand for charging and discharging respectively.

further lead to a rise in resistance and capacity degradation. This forms a vicious cycle that causes the battery to age at increasingly faster rates. The temperature evolution over the simulation period of one year for the 4 batteries is depicted in fig. 7. It is seen that the batteries reach significantly high intermittent temperatures during the operation, which is attributed to the lack of a cooling system in the simulation. In a real-world situation, active cooling measures would be

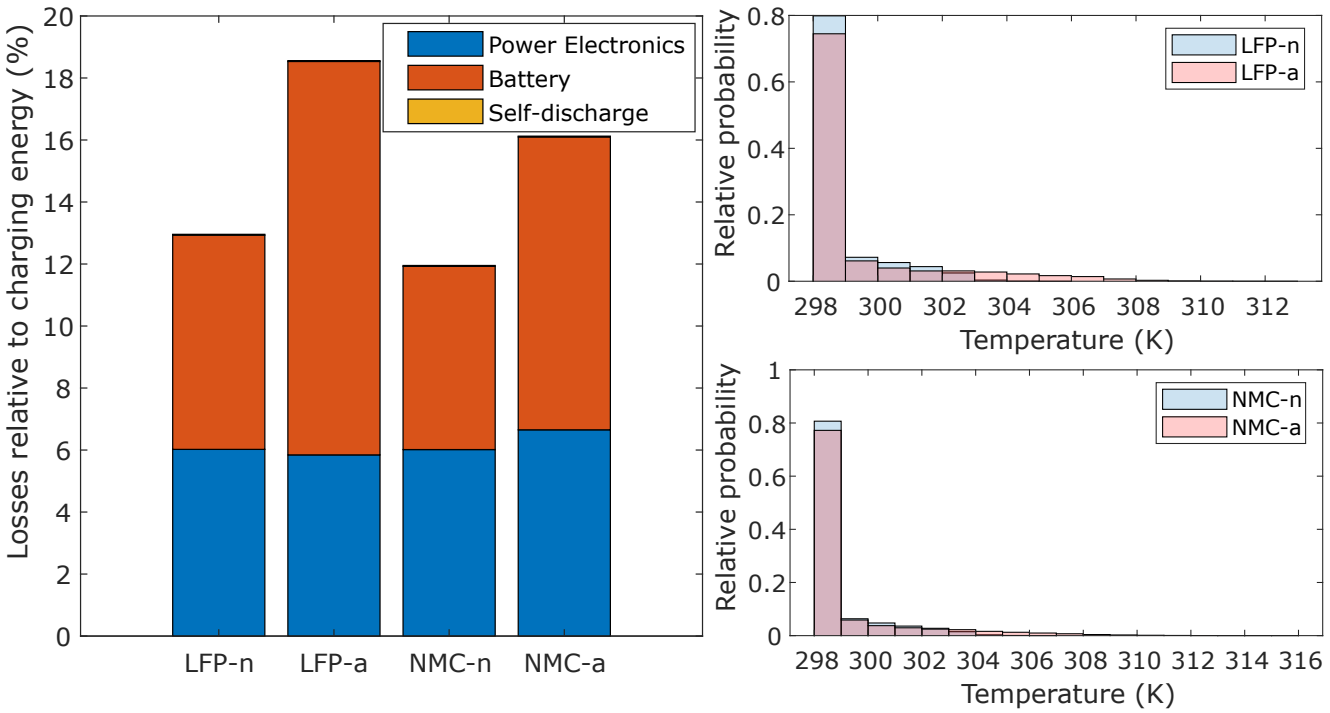

Fig. 7: Conversion losses with new (n) and aged (a) LFP and NMC cells in the peak shaving application (left). Temperature (in K) of simulated cells over duration of simulation in the absence of cooling measures (right).

undertaken by the thermal management system (TMS) to keep the cells within their normal temperature ranges. For the NMC/C cells, the high intermittent temperatures are also attributed to the low specific heat capacity of the cells, which needs further investigation.

With aged batteries, it is of particular interest to investigate if the system availability is maintained despite the faded capacity and higher resistance. As the chosen application does not exhibit very wide peaks which need to be shaved, the battery system does not undergo high depth-of-discharge (DOD) cycles. As a result, the lower capacity of the batteries does not impede the system availability. The lower terminal voltage due to the increased resistance also does not affect the system availability, as the batteries are able to supply power at higher currents to meet the power request at a lower terminal voltage. This results in even higher battery conversion losses, which is apparent from figure 7.

C. Power electronics

Several power electronics topologies are used to interface the battery system to the grid. The most common among these, depending on whether there is a DC/DC voltage conversion stage between the batteries and the AC/DC conversion, are termed as single-stage and the two-stage topologies [17], [44]. Load distribution strategies also play an important role in the final choice of the power electronics components used and their interconnection. While some systems rely on load distribution strategies which do not introduce large SOC deviations among strings, some [45] rely on strategies that actively balance the widely divergent SOCs by distributing the power dynamically among the strings.

The inverter/rectifier model used for simulations in this work is based on a full characterization of a commercially available bi-directional converter such that the losses in both directions at various load levels are modeled in the form of a look-up table [14]. Scaling factors are used to adjust the model to the power rating of simulated system. The PE topology used to simulate the BESS operation in section IV-A is depicted in fig. 8. In this topology, each battery string is connected to a separate bidirectional AC/DC converter. The load distribution strategy operates the individual converters such that the power demand at the system coupling point is uniformly fulfilled by all the strings. For this topology the following relations hold true:

$$P_{nominal,sys} = n * P_{nominal,converter} \tag{7a}$$

$$P_{t,sys} = x * n * P_{nominal,converter} \tag{7b}$$

$$0 \leq x \leq 1 \tag{7c}$$

where:
.. $P_{nominal,sys}$ is the rated power of the system
.. $P_{nominal,converter}$ is the rated power of each individual converter
.. n is the total number of converters in the topology
.. x is the load factor at time t

To illustrate the effect of the power electronics topology on the system conversion efficiency, the 15^{th} of July (depicted in fig. 5), representing the worst case among the 12 days

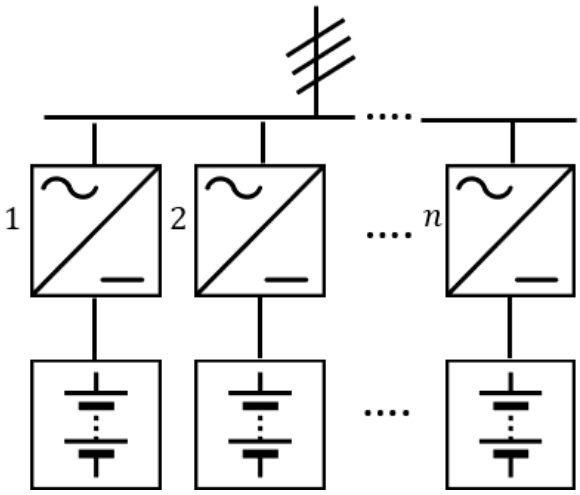

Fig. 8: Dedicated string converter topology operating with the uniform load distribution strategy.

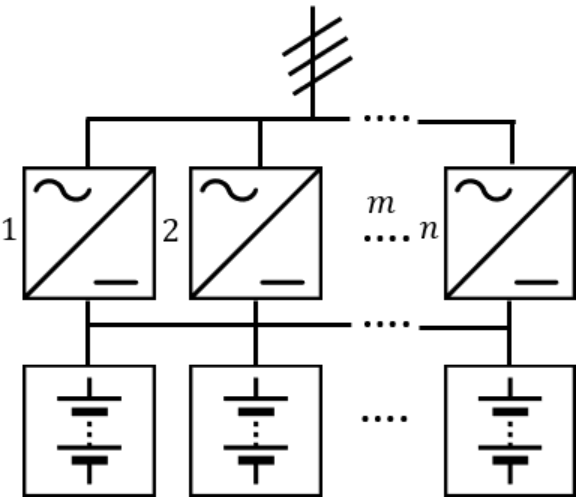

Fig. 9: Converter topology with common DC bus operating with the incremental load distribution strategy.

simulated, is considered as a base case. It has been discussed that these high conversion losses are caused due to prolonged part-load operation. A second converter topology, in which all the battery strings are connected in parallel to the array of AC/DC bidirectional converters is now considered. The strings no longer possess dedicated converters in this topology, but there are now several converters which can be sequentially brought online to match the power demand. This topology is depicted in figure 9. For this topology, the following relations for the system power hold true:

$$P_{nominal,sys} = n * P_{nominal,converter} \tag{8a}$$

$$P_{t,sys} = m * P_{nominal,converter} + x * P_{nominal,converter} \tag{8b}$$

$$0 \leq m \leq n \tag{8c}$$

$$0 \leq x \leq 1 \tag{8d}$$

where:
.. m is the number of converters being operated at the specified upper threshold
.. x is the load factor of the $(m+1)^{th}$ converter at time t

It is important to state here that the relations presented in equations (7) and (8) are valid if all the individual converters are identical. For the case with dissimilar converters, the equations can still be used with some minor adjustments.

Schimpe et al [17] have evaluated the relative losses arising due to the operation of the grid coupling components namely the DC/DC bidirectional converter, AC/DC bidirectional converter and the transformer. Two-stage and single stage topologies are also evaluated, with the incremental topology investigated in connection to a prototype system. A simulation framework has been developed to investigate the effect of such an incremental inverter topology on the system conversion efficiency with a variable number of converters. The chosen base case is now simulated with the topology depicted in fig. 9, with the number of inverters n being varied from 2 to 10. For the base case simulated earlier, $n = 1$. As can be seen in figure 11, the additional benefit of each extra inverter diminishes with the number of inverters, while the mean conversion efficiency across the power range (shown on the secondary y-axis) eventually flattens out. While these results may make it seem like it is in the system designer's interest to keep increasing the number of converters indefinitely to obtain even better mean efficiencies, caution is advised due to the likeliness of the economic and environmental costs per kW of rated capacity making such an implementation prohibitive. Which implies monetary and energetic gains in efficiency, could be nullified due to higher investment costs of BOS components. A comprehensive and focused analysis of these questions needs to be carried out in order to arrive at a clearer conclusion. The conversion efficiency curve for the topology depicted in figure 9, operating under the incremental load distribution strategy is calculated across the entire load range. Efficiency curves for topologies consisting of 1 to 10 converters are depicted in figure 10. The efficiency values for all cases converge towards the end of the power range as then all converters are operating at rated power. The deployment of such a topology yields the best results during operation at low relative power values.

V. Conclusion and outlook

Rising electricity production from variable renewable energy sources such as solar and wind energy, while making the energy from the world's most versatile energy vector greener, has also brought unique challenges into the picture which, if not addressed in a timely fashion, threaten the quality and security of power supply across the world. Lithium-ion battery energy storage systems, the technology which is expected to provide relief to the systems need to be designed and analyzed comprehensively to equip them better to tackle the challenges efficiently and effectively. It has been shown how the conversion efficiencies of the major components of a BESS

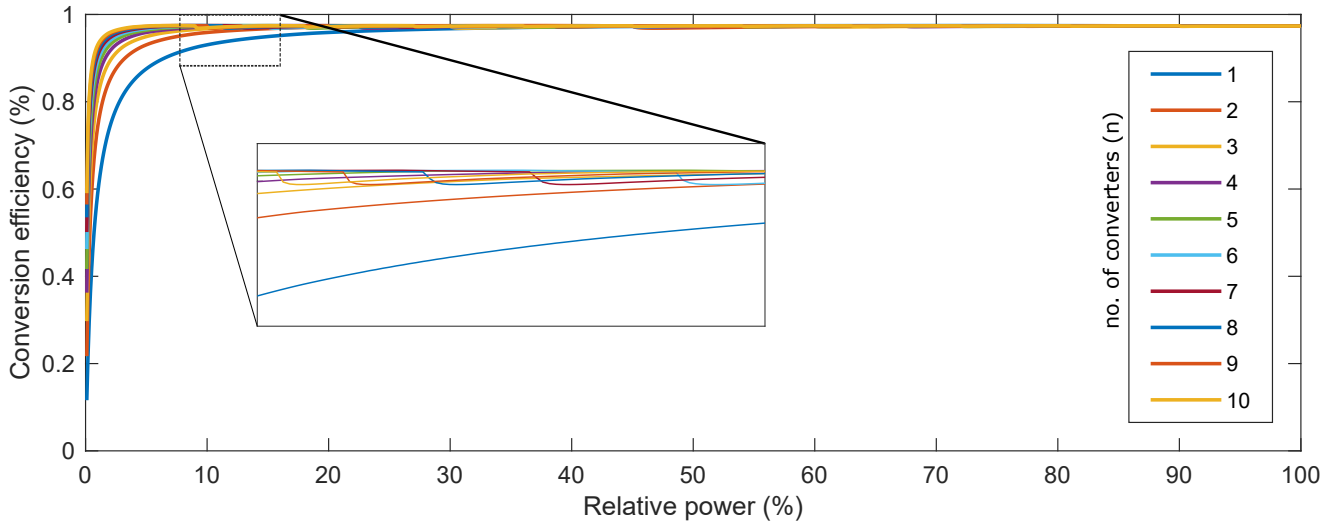

Fig. 10: Efficiency curves for the topology with incremental load distribution strategy (for topologies with number of converters $n = 1$ to $n = 10$). The inset image depicts the second and third converters C2 and C3 respectively coming online for a topology with 10 converters.

.

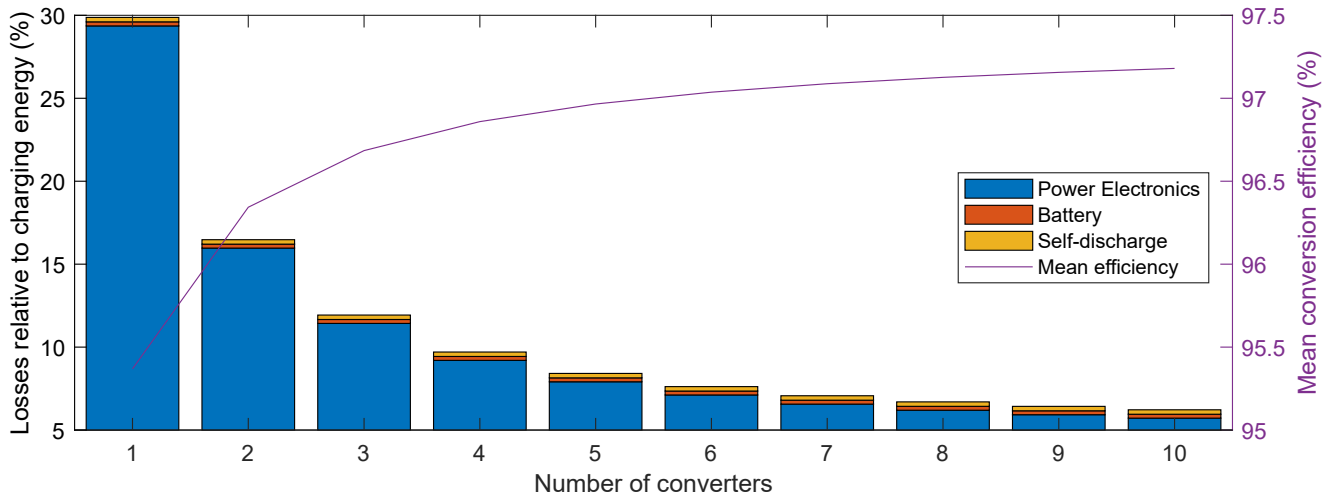

Fig. 11: Reduction in conversion losses in power electronics for the worst case by increasing the number of converters (stacked bar graph, left axis). Mean conversion efficiency of topology across load range (line graph, right axis).

- the power electronics and the batteries play a major role in the overall round trip efficiency of the system. It is also clear that the system losses need to be studied and modeled further in a holistic manner in order to be able to evaluate and quantify these losses for stationary BESS with minimal effort. Power electronics topologies, the type of coupling with the batteries, and their load distribution strategies are instrumental in certain applications with lower average C-rates, while being of lesser significance in others with higher average C-rates. It has also been shown how the possible usage of second-life batteries can affect the system efficiency and availability in particularly demanding applications such as peak shaving. It is imperative to mention here that aged batteries are not always able to shave off some of the highest and widest peaks completely due to the rise in resistance and degradation in capacity over time. A thorough investigation into the sizing methodologies for second-life batteries in existing applications in order to ensure maximum possible system availability is also necessary.

Based on the area of interest and the properties to be investigated, there are a variety of models in use today which simulate the electrochemical, thermal, mechanical and energetic performance [46]. System level stationary BESS models with varying levels of details have been proposed in the literature [47], which aim to address the scaling up

of the system from a single cell model to a module and rack level model. These models focus primarily on the core component of the BESS, which is the battery system and the battery management system (BMS). The power electronics and the auxiliary components such as the energy management system (EMS), the thermal management system (TMS) are not coupled to the core battery system, consequently the influence thereof is not immediately apparent. Other models [14] which include the auxiliary components do not address the complexities encountered in the scaling process to keep the computational effort within acceptable bounds. A holistic system model framework is needed to provide a rigorous treatment to each aspect of the stationary BESS. Such a framework will not only enable faster design and development of Lithium-ion battery energy storage systems, but also the analysis of the influence of variation in application scenarios, individual sub-system configurations and attributes on the overall system efficiency. The economic and environmental appeal of stationary energy storage systems as a viable technology to support further integration of renewable energy sources into the energy system can be enhanced with such evaluations. The authors intend to take a closer look at the aforementioned areas of research in subsequent works.

VI. Acknowledgments

This research is funded by the German Federal Ministry for Economic Affairs and Energy (BMWi), via the research project EffSkalBatt (grant number 03ET6148A), and overseen by Project Management Juelich (PtJ). The authors would also like to thank Daniel Kucevic for making the PCR load profile available, and Yulong Zhao, who helped implement the NMC/C model in SimSES. Stefan Englberger provided us with some of his self-created graphic symbols. The sankey diagram plotting tool for MATLAB has been created by James Spelling [48]. The cliparts in figure 1 were created by their respective owners [49].

References

[1] Harry Wirth. Recent facts about photovoltaics in germany.

[2] Rebecca Jones-Albertus, David Feldman, Ran Fu, Kelsey Horowitz, and Michael Woodhouse. Technology advances needed for photovoltaics to achieve widespread grid price parity. *Progress in Photovoltaics: Research and Applications*, 24(9):1272–1283, 2016.

[3] Ranjit Deshmukh, Grace C. Wu, Duncan S. Callaway, and Amol Phadke. Geospatial and techno-economic analysis of wind and solar resources in india. *Renewable Energy*, 134:947–960, 2019.

[4] Amirhossein Sajadi, Luka Strezoski, Vladimir Strezoski, Marija Prica, and Kenneth A. Loparo. Integration of renewable energy systems and challenges for dynamics, control, and automation of electrical power systems. *Wiley Interdisciplinary Reviews: Energy and Environment*, 8(1):e321, 2019.

[5] William Zappa, Martin Junginger, and Machteld van den Broek. Is a 100% renewable european power system feasible by 2050? *Applied Energy*, 233-234:1027–1050, 2019.

[6] J. Cochran, M. Miller, O. Zinaman, M. Milligan, D. Arent, B. Palmintier, M. O'Malley, S. Mueller, E. Lannoye, A. Tuohy, B. Kujala, M. Sommer, H. Holttinen, J. Kiviluoma, and S. K. Soonee. Flexibility in 21st century power systems.

[7] Michael Child, Claudia Kemfert, Dmitrii Bogdanov, and Christian Breyer. Flexible electricity generation, grid exchange and storage for the transition to a 100% renewable energy system in europe. *Renewable Energy*, 139:80–101, 2019.

[8] Patrick T. Moseley and Jürgen Garche. *Electrochemical energy storage for renewable sources and grid balancing*. Elsevier, Amsterdam, 2015.

[9] Holger Hesse, Michael Schimpe, Daniel Kucevic, and Andreas Jossen. Lithium-ion battery storage for the grid—a review of stationary battery storage system design tailored for applications in modern power grids. *Energies*, 10(12):2107, 2017.

[10] Furquan Nadeem, S. M. Suhail Hussain, Prashant Kumar Tiwari, Arup Kumar Goswami, and Taha Selim Ustun. Comparative review of energy storage systems, their roles, and impacts on future power systems. *IEEE Access*, 7:4555–4585, 2019.

[11] Ruben Hidalgo-Leon, Diego Siguenza, Carola Sanchez, Jonathan Leon, Pablo Jacome-Ruiz, Jinsong Wu, and Diego Ortiz. A survey of battery energy storage system (bess), applications and environmental impacts in power systems. In *2017 IEEE Second Ecuador Technical Chapters Meeting (ETCM)*, pages 1–6. IEEE, 16.10.2017 - 20.10.2017.

[12] Aoxia Kevin Chen, Yaswanth Nag Velaga, and Pankaj K. PK. Sen. Future electric power grid and battery storage. In *2019 IEEE Texas Power and Energy Conference (TPEC)*, pages 1–6. IEEE, 07.02.2019 - 08.02.2019.

[13] G. Pistoia. *Lithium-ion batteries: Advances and applications / [editor] Gianfranco Pistoia*. Elsevier, Amsterdam, first edition edition, 2014.

[14] Michael Schimpe, Maik Naumann, Nam Truong, Holger C. Hesse, Shriram Santhanagopalan, Aron Saxon, and Andreas Jossen. Energy efficiency evaluation of a stationary lithium-ion battery container storage system via electro-thermal modeling and detailed component analysis. *Applied Energy*, 210:211–229, 2018.

[15] Cong Nam Truong, Michael Schimpe, Maik Naumann, Andreas Jossen, and Holger C. Hesse. Impact of sub-components on the overall performance of stationary battery systems: Insights on the prototype energy neighbor: 28-29 nov. 2017. 2017.

[16] Charalampos Patsios, Billy Wu, Efstratios Chatzinikolaou, Daniel J. Rogers, Neal Wade, Nigel P. Brandon, and Phil Taylor. An integrated approach for the analysis and control of grid connected energy storage systems. *Journal of Energy Storage*, 5:48–61, 2016.

[17] Michael Schimpe, Nick Becker, Taha Lahlou, Holger C. Hesse, Hans-Georg Herzog, and Andreas Jossen. Energy efficiency evaluation of grid connection scenarios for stationary battery energy storage systems. *Energy Procedia*, 155:77–101, 2018.

[18] Helder Lopes Ferreira, Raquel Garde, Gianluca Fulli, Wil Kling, and Joao Pecas Lopes. Characterisation of electrical energy storage technologies. *Energy*, 53:288–298, 2013.

[19] Maik Naumann. *Techno-economic evaluation of stationary battery energy storage systems with special consideration of aging*. Doctoral, 2018.

[20] Rodrigo Martins, Holger Hesse, Johanna Jungbauer, Thomas Vorbuchner, and Petr Musilek. Optimal component sizing for peak shaving in battery energy storage system for industrial applications. *Energies*, 11(8):2048, 2018.

[21] Alexandre Oudalov, Rachid Cherkaoui, and Antoine Beguin. Sizing and optimal operation of battery energy storage system for peak shaving application. In *2007 IEEE Lausanne Power Tech*, pages 621–625. IEEE, 01.07.2007 - 05.07.2007.

[22] Jason Leadbetter and Lukas Swan. Battery storage system for residential electricity peak demand shaving. *Energy and Buildings*, 55:685–692, 2012.

[23] O. Veneri, L. Ferraro, C. Capasso, and D. Iannuzzi. Charging infrastructures for ev: Overview of technologies and issues. In *2012 Electrical Systems for Aircraft, Railway and Ship Propulsion*, pages 1–6. IEEE, 16.10.2012 - 18.10.2012.

[24] Daniel-Ioan Stroe, Vaclav Knap, Maciej Swierczynski, Ana-Irina Stroe, and Remus Teodorescu. Operation of a grid-connected lithium-ion battery energy storage system for primary frequency regulation: A battery lifetime perspective. *IEEE Transactions on Industry Applications*, 53(1):430–438, 2017.

[25] Johannes Fleer and Peter Stenzel. Impact analysis of different operation strategies for battery energy storage systems providing primary control reserve. *Journal of Energy Storage*, 8:320–338, 2016.

[26] Maciej Swierczynski, Daniel Ioan Stroe, Ana Irina Stan, and Remus Teodorescu. Primary frequency regulation with li-ion battery energy storage system: A case study for denmark. In *2013 IEEE ECCE Asia Downunder*, pages 487–492. IEEE, 03.06.2013 - 06.06.2013.

[27] Yann G. Rebours, Daniel S. Kirschen, Marc Trotignon, and Sbastien Rossignol. A survey of frequency and voltage control ancillary

services—part i: Technical features. *IEEE Transactions on Power Systems*, 22(1):350–357, 2007.
[28] Yann G. Rebours, Daniel S. Kirschen, Marc Trotignon, and Sbastien Rossignol. A survey of frequency and voltage control ancillary services—part ii: Economic features. *IEEE Transactions on Power Systems*, 22(1):358–366, 2007.
[29] ENTSO - E. Operations handbook.
[30] Maik Naumann, Cong Nam Truong, Michael Schimpe, Daniel Kucevic, Andreas Jossen, and Holger C. Hesse. *SimSES: Software for techno-economic Simulation of Stationary Energy Storage Systems: 28-29 November 2017*. VDE, Berlin, Germany, 2018.
[31] Simon F. Schuster, Martin J. Brand, Christian Campestrini, Markus Gleissenberger, and Andreas Jossen. Correlation between capacity and impedance of lithium-ion cells during calendar and cycle life. *Journal of Power Sources*, 305:191–199, 2016.
[32] E. Peter Roth. Thermal abuse performance of moli, panasonic and sanyo 18650 li-ion cells: Final report to nasajsc.
[33] Jinhao Meng, Guangzhao Luo, Mattia Ricco, Maciej Swierczynski, Daniel-Ioan Stroe, and Remus Teodorescu. Overview of lithium-ion battery modeling methods for state-of-charge estimation in electrical vehicles. *Applied Sciences*, 8(5):659, 2018.
[34] Fida Saidani, Franz X. Hutter, Rares-George Scurtu, Wolfgang Braunwarth, and Joachim N. Burghartz. Lithium-ion battery models: a comparative study and a model-based powerline communication. *Advances in Radio Science*, 15:83–91, 2017.
[35] J. Li, N. Lotfi, R. G. Landers, and J. Park. A single particle model for lithium-ion batteries with electrolyte and stress-enhanced diffusion physics. *Journal of The Electrochemical Society*, 164(4):A874–A883, 2017.
[36] Hongwen He, Rui Xiong, and Jinxin Fan. Evaluation of lithium-ion battery equivalent circuit models for state of charge estimation by an experimental approach. *Energies*, 4(4):582–598, 2011.
[37] Alexandros Nikolian, Joris de Hoog, Karel Fleurbay, Jean-Marc Timmermans, Omar Noshin, Peter van de Bossche, and Joeri van Mierlo. Classification of electric modelling and characterization methods of lithium-ion batteries for vehicle applications. 2014.
[38] Dian Wang, Yun Bao, and Jianjun Shi. Online lithium-ion battery internal resistance measurement application in state-of-charge estimation using the extended kalman filter. *Energies*, 10(9):1284, 2017.
[39] Johannes Schmalstieg, Stefan Käbitz, Madeleine Ecker, and Dirk Uwe Sauer. A holistic aging model for li(nimnco)o2 based 18650 lithium-ion batteries. *Journal of Power Sources*, 257:325–334, 2014.
[40] Madeleine Ecker, Nerea Nieto, Stefan Käbitz, Johannes Schmalstieg, Holger Blanke, Alexander Warnecke, and Dirk Uwe Sauer. Calendar and cycle life study of li(nimnco)o2-based 18650 lithium-ion batteries. *Journal of Power Sources*, 248:839–851, 2014.
[41] Noshin Omar, Mohamed Abdel Monem, Yousef Firouz, Justin Salminen, Jelle Smekens, Omar Hegazy, Hamid Gaulous, Grietus Mulder, Peter van den Bossche, Thierry Coosemans, and Joeri van Mierlo. Lithium iron phosphate based battery – assessment of the aging parameters and development of cycle life model. *Applied Energy*, 113:1575–1585, 2014.
[42] Maik Naumann, Michael Schimpe, Peter Keil, Holger C. Hesse, and Andreas Jossen. Analysis and modeling of calendar aging of a commercial lifepo4/graphite cell. *Journal of Energy Storage*, 17:153–169, 2018.
[43] M. Schimpe, M. E. von Kuepach, M. Naumann, H. C. Hesse, K. Smith, and A. Jossen. Comprehensive modeling of temperature-dependent degradation mechanisms in lithium iron phosphate batteries. *Journal of The Electrochemical Society*, 165(2):A181–A193, 2018.
[44] Sergio Vazquez, Srdjan M. Lukic, Eduardo Galvan, Leopoldo G. Franquelo, and Juan M. Carrasco. Energy storage systems for transport and grid applications. *IEEE Transactions on Industrial Electronics*, 57(12):3881–3895, 2010.
[45] Michael Schimpe, Christian Piesch, Holger Hesse, Julian Paß, Stefan Ritter, and Andreas Jossen. Power flow distribution strategy for improved power electronics energy efficiency in battery storage systems: Development and implementation in a utility-scale system. *Energies*, 11(3):533, 2018.
[46] Venkatasailanathan Ramadesigan, Paul W. C. Northrop, Sumitava De, Shriram Santhanagopalan, Richard D. Braatz, and Venkat R. Subramanian. Modeling and simulation of lithium-ion batteries from a systems engineering perspective. *Journal of The Electrochemical Society*, 159(3):R31–R45, 2012.
[47] Matthieu Dubarry, George Baure, Carlos Pastor-Fernández, Tung Fai Yu, W. Dhammika Widanage, and James Marco. Battery energy storage system modeling: A combined comprehensive approach. *Journal of Energy Storage*, 21:172–185, 2019.
[48] James Spelling. drawsankey function for matlab, available on matlab central. access link: https://ch.mathworks.com/matlabcentral/fileexchange/26573-drawsankey.
[49] Freepik, Pause08, Eucalyp, and Smashicons. Cliparts from www.flaticon.com. licensed with creative commons by3.0.